RESEARCH ARTICLE | JULY 25 2009

Ultrafast Space-time and Spectrum-time Resolved Diagnostics of Multicharged Femtosecond Laser Microplasma

S. V. Garnov; V. V. Bukin; A. A. Malyutin; ... et. al

AIP Conference Proceedings 1153, 37–48 (2009)
https://doi.org/10.1063/1.3204548

Ultrafast Space-time and Spectrum-time Resolved Diagnostics of Multicharged Femtosecond Laser Microplasma

S. V. Garnov, V. V. Bukin, A. A. Malyutin and V. V. Strelkov

A.M. Prokhorov General Physics Institute of Russian Academy of Sciences
119991, Vavilov str. 38, Moscow, Russia; garnov@kapella.gpi.ru

Abstract. We present the review of the recent experimental studies of fundamental mechanisms of femtosecond laser plasma formation and evolution performed in A.M. Prokhorov General Physics Institute of Russian Academy of Sciences. The main object we dealt with was the micro-sized plasma produced in gases with high intensity (up to 5×10^{17} W/cm^2), tightly focused (to a few microns in diameter) IR and UV femtosecond laser pulses. The main attention in the experiments was paid to the initial stage of microplasma formation and evolution characterized by strong laser-plasma coupling resulting in efficient ionization and heating of the medium, distortion of laser beam, and nonlinear spectral conversion of laser radiation to the continuum and laser harmonics. Using a precise pump-probe micro-interferometric technique the dynamics of plasma was studied with femtosecond time-resolution in a wide density range - from a minimal detectable electron concentration (10^{19} cm^{-3}) to the almost total (down to nuclei) ionization of ions occurred under femtosecond excitation. The obtained time-dependences of plasma density were analyzed. It was observed, for the first time, that a characteristic time of femtosecond laser plasma formation in gases considerably (in times) exceeds the duration of the pump laser pulse. This *postionization* process is attributed to impact ionization of plasma by hot electrons. We compare the results of the experiments with what the developed theory predicts. Using an ultrafast streak-camera-based spectroscopy technique the temporal evolution of microplasma emission and the dynamics of spectral lines formation in UV-visible range were studied with picosecond time-resolution.

Keywords: Femtosecond Laser Microplasma, Pump-probe Interferometry, Ultrafast Spectroscopy, Electron Density, Postionization.
PACS: 52.38.-r; S32.80.Fb; M32.80.Rm; 42.30.Rx

INTRODUCTION

The study of nonequilibrium laser plasma produced in gases by high intensity ultrashort laser pulses is one of the clue tasks of laser-matter interaction physics. This problem is topical both for fundamental science and for numerous applications. Among them are: an acquiring new basic knowledge on the properties of extremely nonequilibrium high-density plasma and the mechanisms of plasma formation, evolution and interaction with laser radiation; development of techniques for the generation of extremely short (attosecond) light pulses; development of laser-driven sources of X-ray and UV radiation for nanolithography, etc. In this work, we report on the experimental investigations of ultrafast formation and evolution of laser plasmas produced in microvolumes of gases (air, nitrogen, argon, helium) by tightly focused

CP1153, *Laser-Driven Relativistic Plasmas Applied to Science, Industry and Medicine - The 2nd International Symposium*
edited by P. R. Bolton, S. V. Bulanov, and H. Daido

(to a several microns), high intensity (from ~10^{14} W/cm^2 to ~5×10^{17} W/cm^2) femtosecond pulses of Ti:Sa laser. Such a plasma with a characteristic diameter of several microns and a length up to several tens of microns (the so-called *microplasma*) is an interesting and important object for experimental investigations both in view of the aforementioned basic and applied aspects of this problem and in connection with the unique opportunity to study the behavior of matter and plasma in superstrong laser fields (of sub-relativistic intensities) employing relatively simple and compact femtosecond laser facilities. Indeed, a typical quality of Ti:Sa laser beam permits focusing it to a region of about 1 μm in diameter and thereby attaining 'in-vacuum' intensities as high as 10^{18} W/cm^2 even for a pulse energy of 1 mJ and a laser pulsewidth of 100 fs. Therefore, the microplasma production by high-intensity femtosecond pulses in itself presents no special problems. However the study of microplasma may encounter serious experimental obstacles and, in the first place, the inadequate readiness of the methods for the investigation of transient *microdimensional* plasma objects and the ultrafast physical processes occurring therein, including the methods of ultrafast laser microinterferometry and ultrafast spectroscopy. In this work we present the results of our investigations aimed at the development and practical realization of the methods for microplasma studies. Earlier we reported on the techniques for precision microinterferometry of microplasma generated in gases and optical media (quartz) by picosecond laser pulses [1,2]. More recently these techniques were substantially modified and employed to investigate femtosecond microplasmas [3,4]. In addition we proposed a method for ultrafast electro-optical recording the emission spectra of laser-produced microplasma [3,5-7].

PUMP-PROBE INTERFEROMETRY OF FEMTOSECOND LASER MICROPLASMA

Experimental Arrangements

The experimental setup used for pump-probe interferometric measurements of femtosecond laser microplasma formation and evolution is shown in Fig. 1. A single 100 fs pulse from a Ti:Sa laser (*Spectra-Physics*) was split into two unequal parts - the high intensity exciting (pump) pulse and the low intensity probe pulse. After conversion to the second harmonic in a thin KDP (or a BBO) crystal, the pump pulse was focused into the volume of gas to ionize it and thus to produce a microplasma. Focusing was performed with a high-quality aspheric lens (F=8 mm; NA=0.5). The inset in Fig. 1 shows the measured spatial intensity profile of the focused laser pulse. One can see that the intensity distribution near the focal plane is close to the Gaussian one with a diameter of 1.7 μm (at the 1/e^2 level).

The conversion of the fundamental laser harmonic (λ=800 nm) to the second one (λ=400 nm) allowed us to enhance considerably the laser intensity contrast ratio, which is very important in investigations of plasma produced by laser pulses with peak intensities of 2-3 orders of magnitude higher than the gas optical breakdown threshold (which is typically ~10^{14} W/cm^2 for the air, nitrogen, and argon).

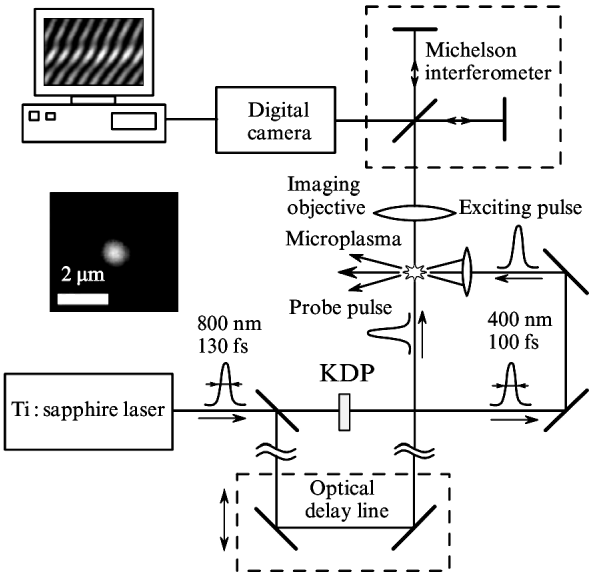

FIGURE 1. Schematic drawing of the experimental setup used for interferometric measurements of femtosecond laser microplasma formation and evolution. Inset: the spatial profile of laser intensity distribution measured in the focal plane of focusing lens.

Because the contrast ratio for the fundamental harmonic radiation measured with a standard correlator was no less than 100:1, after the conversion to the second harmonic it increased quadratically to more than 1000:1. This allowed us to eliminate (or at least to minimize) the effect of a low-intensity pedestal and pre- and post-pulses, which are always present in the fundamental output radiation of femtosecond lasers. After reflection from the beamsplitter, the probe pulse passed through a variable optical time-delay line and propagated through the plasma under study perpendicular to the pump pulse path. By varying the length of the delay line by a precision step motor, we changed the arrival time of the probe pulse to the plasma relative to the pump pulse. The time-tuning range was 0 - 40 ps with a minimal step of 10 fs. The fundamental harmonic of the Ti:Sa laser (λ=800 nm) was used for probe plasma to provide the highest possible sensitivity of measuring low electron densities. After passing the plasma the probe pulse was collected by an imaging objective (F=50 mm, NA=0.5) and directed to a Michelson interferometer which divided the probe radiation into two coherent beams propagating at a small angle. Because the dimensions of the microplasma were much smaller than the probe-pulse diameter (~3 mm), its main part propagated outside the region of induced optical inhomogeneity could be used as a reference beam. In this case, the Michelson interferometer was used to separate the reference and object beams, to select the orientation and period of interference fringes, and to compensate for the path difference of the interfering femtosecond pulses. Recall that all numerous pulsed laser interferometric techniques for plasma diagnostics, which have been used many times earlier and are presently used in numerous experimental works (see for instance, [1-28] and references therein), are based on the

recording of the 'instantaneous' interference patterns of the volume of the excited matter (plasma), which are obtained with the help of probe laser 'illumination' pulses delayed in time. A bending of fringes in the interference patterns corresponds to the phase shift of the probe pulse immediately after its passage through the microplasma (a shift by one fringe corresponds to a phase shift of 2π). The spatial distribution of the phase shift of the probe pulse was reconstructed on the basis of the standard Fourier filtration algorithm [29, 30]. In this case, the sensitivity of phase shift measurement (in our case about $2\pi/30$ - $2\pi/500$), far exceeds the sensitivity of the 'spatial' method involving the determination of interference fringe coordinates. The phase of the probe pulse changes due to a change in the refractive index inside the microplasma relative to the refractive index of the unperturbed gas. For a cylindrical symmetry of the plasma object, this change is related to the refractive index distribution by the Abelian transformation. Accordingly, by using the inverse Abelian transformation it is possible to obtain the radial dependence of the refractive index distribution inside the microplasma from the spatial distribution of the phase shift. Because the experimentally recorded profiles of the phase shift are always a bit asymmetric, we employed a symmetrisation procedure using the least squares technique. Within the framework of the Drude model, the refractive index n and the electron density N_e are related by the expression [1-4, 31-32]:

$$n(r,t) = \sqrt{n_0^2 - \left(\frac{\omega_p(r,t)}{\omega}\right)^2}\ ,\ \omega_P^2(r,t) = \frac{N_e(r,t)\cdot e^2}{\varepsilon_0 \cdot m_e}, \qquad (1)$$

where $\omega=2.35\times10^{15}$ rad/s is the angular frequency of the probe radiation; ω_p is the plasma frequency; e and m_e are the electron charge and mass; and ε_0 is the dielectric constant. Thus, proceeding from the 'instantaneous' interference patterns of the laser plasma, we obtained the 'instantaneous' spatial distributions of the electron density inside the microplasma.

Experimental Results

The air, nitrogen, argon, and helium gas plasmas were studied by focusing the laser pulse into a slow-speed gas jet at the atmospheric pressure. The stages of interference pattern processing listed above are represented in Fig. 2. The interference patterns were processed by using the freely distributed software *IDEA* (*Interferometric Data Evaluation Algorithms*; http://www.optics.tugraz.at/idea/idea.html). Fig. 3a presents the electron density data for nitrogen and argon microplasmas measured near the focus in the 0-5000 fs time range. One can see that the characteristic time of fast plasma formation is about 500 fs; then, the growth in the electron density slows down but does not terminate completely. It is also evident that the duration of the stage of a rapid growth of the electron density virtually corresponds to the duration of laser action, which is determined in this case by the time during which the laser radiation intensity exceeds the threshold intensity of the gas breakdown. For a Gaussian temporal profile, the peak intensity $I = 4\times10^{16}$ W/cm^2, and the breakdown threshold $I_{th} \sim 10^{14}$ W/cm^2 (nitrogen), the duration of 'pump laser action' is about 300 fs. For a helium plasma (Fig. 3b), the duration of rapid plasma formation also corresponds to

the time of laser action. The relatively wide scatter in data points is due to the low (at the limit of sensitivity of our technique) electron density of this plasma.

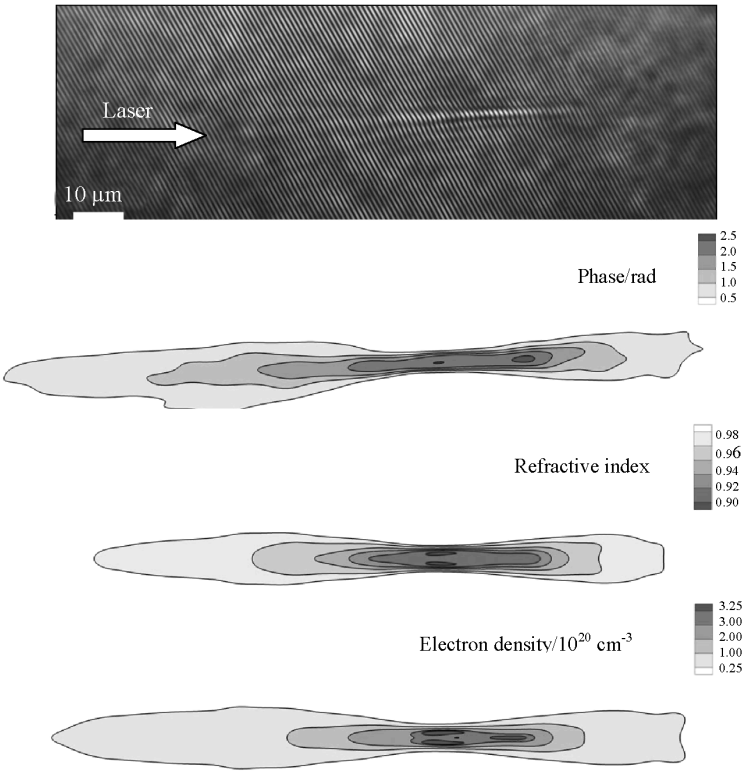

FIGURE 2. Interferogram and spatial distributions of probe pulse phase shift, refractive index and electron density of air microplasma (the probe pulse time delay is 10 ps; the peak intensity of the exciting pulse is 10^{16} W/cm^2).

One can see from Fig. 3b that upon the optical breakdown of helium under these conditions, the electron plasma density achieves its maximum possible value (doubly ionised helium) in less than 500 fs and then ceases to build up. However, for nitrogen, as follows from Fig. 3a, the electron plasma density continues to increase for a substantially longer time - for several picoseconds, which exceeds the period of plasma interaction with the exciting laser radiation. As far as is known from the literature, earlier this process has never been observed experimentally in the femtosecond laser plasma created at optical breakdown of gaseous media.

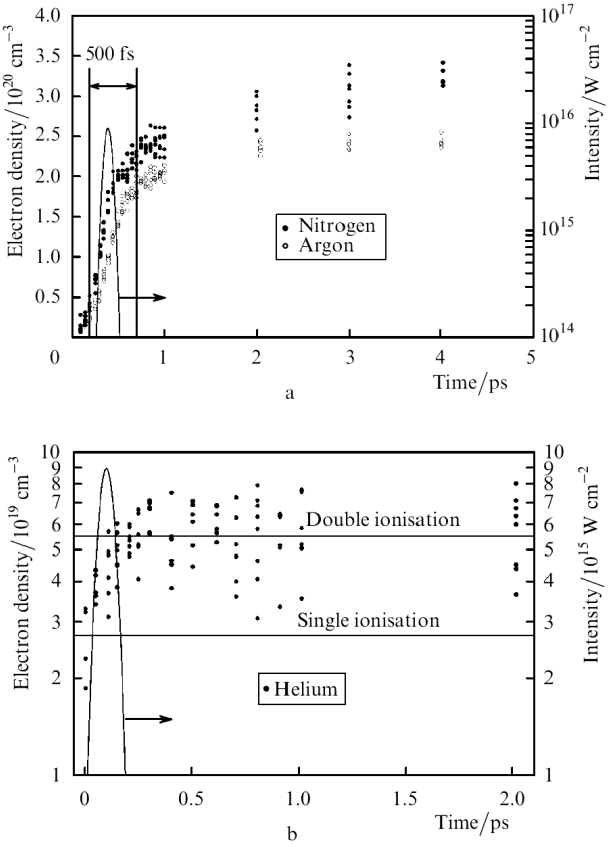

FIGURE 3. Time dependences of plasma electron density measured at the center of beam waist in nitrogen and argon (a) and in helium (b). The temporal intensity profile of 100-fs Gaussian pump pulse with the peak intensity 10^{16} W/cm^2 is shown as the solid curve.

Theory of Microplasma Formation and Evolution

We consider the following gas/plasma ionization mechanisms: the laser pump pulse ionizes the gas and heats the released photoelectrons and then the collisional ionization of ions by hot photoelectrons occurs. The calculated electron density dynamics based on this mechanisms are consistent with the experimental data. The calculation procedure is briefly described below.

Photoionization. The photoionization rate for an atom or an ion with a charge Z and ionization potential I_Z placed in the electric field $E(t)$ is expressed as [32]:

$$w_Z(t) = \frac{4m^3|e|^9 E_Z}{E(t)\hbar^7}\exp\left[-\frac{2m^2|e|^5 E_Z}{3E(t)\hbar^4}\right],\ E_Z = \left(I_Z/Ry\right)^{3/2}, \qquad (2)$$

were Ry is Rydberg constant. Note that a direct comparison of calculations made by the Eq. 2 with the results of direct numerical integration of the Schrödinger equation performed in [33] demonstrates a high accuracy of the analytical formula. The

densities of atoms $N_0(t)$ and ions $N_Z(t)$ are calculated by integrating numerically the system of rate equations:

$$\begin{aligned} \frac{dN_0}{dt} &= -N_0(t)w_0(t) \\ \frac{dN_1}{dt} &= N_0(t)w_0(t) - N_1(t)w_1(t) \\ &\cdots \\ \frac{dN_Z}{dt} &= N_{Z-1}(t)w_{Z-1}(t) - N_Z(t)w_Z(t) \end{aligned} \tag{3}$$

Here, where $N_0(0)$ is the initial atomic density; and $N_Z(0) = 0$ for $Z \geq 1$. This system includes charge states Z up to those whose photoionization probability is negligible. For the simplicity, we analyzed the photoionization dynamics of air by considering only nitrogen and oxygen and neglecting the contributions made by other gases.

Laser heating. Recent investigations [34-37] of electron scattering by ions in the presence of the laser field show that electrons may be efficiently heated, in particular, due to multiple correlated collisions of an electron, oscillating in the laser field with the same ion ('parachute effect'). We determined the electron temperature by using the approximate analytic expression for the heating rate obtained in [36]. The initial temperature was determined from the average electron energy acquired upon photoionization. Note that the heating rate derived in [36] saturates with temperature, and therefore the temperature reached during heating weakly depends on its initial value. Under our conditions, the calculated temperature at the beam focus after the heating was about 0.3 keV.

Electron impact ionization. The electron density dynamics after the laser action can be calculated from the known cross sections and rates of collisional ionization [37-38] and collisional excitation [39-40] for nitrogen atoms and ions. Note that the temperature dependences of the cross sections for ionization and excitation are nonresonant in the electron temperature range under study. That is why the inaccuracy in determining the electron temperature with the help of the analytical theory [36] should not lead to serious errors in the calculation of the dynamics of collisional ionization. A comparison of the cross sections for direct collisional ionization and collisional excitation shows that under our experimental conditions: (i) ionization occurs primarily due to successive excitation rather than direct ionization; (ii) the rate of the successive process is primarily determined by the rate of excitation from the ground state, while the further excitation and ionization proceed faster. For this reason, the collisional ionization is simulated by using two (for each Z value) rates: the rate of excitation from the ground state to an excited state (the state with the highest excitation probability is selected) and the total rate of all transitions from this state. The ionization dynamics calculated upon excitation of air by a 100 fs Gaussian laser pulse for different peak intensities is presented in Fig. 4a. Fig. 4b shows the experimentally measured radial profile of the refractive index of the femtosecond laser nitrogen microplasma at the moment of time 500 fs following the primary gas breakdown ($I = 1.7\times10^{16}$ W/cm^2) and the result of numerical simulation for the same parameters. One can see that the numerical simulation is in good agreement with the experimentally measured values of the electron density.

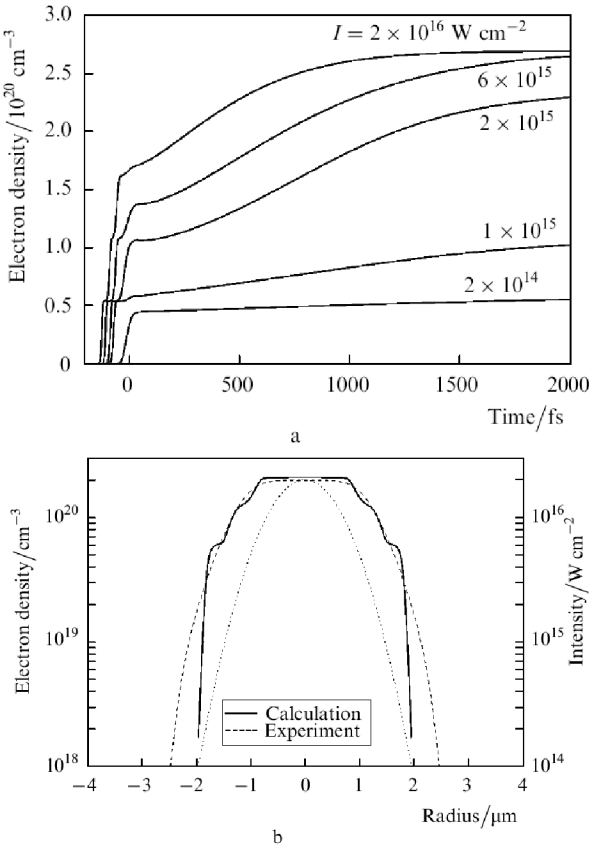

FIGURE 4. Results of numerical calculations of femtosecond air plasma electron density dynamics: the time dependences of the electron density upon excitation by 100-fs Gaussian pulse for different peak intensities (a), and the radial electron density distribution in the beam waist measured experimentally in air 500 fs after the primary gas breakdown (the dashed lined) and calculated theoretically (the solid line) (b). The dotted line shows the radial distribution of the peak laser intensity.

It should be noted that the special features - 'steps', in the calculated profile of the electron density have a characteristic size of less than 0.5 μm, which is substantially smaller than the spatial resolution of our experimental technique. Note that the photo-ionization by the picosecond pedestal or the postpulse may have another explanation for the growth of electron density after the end of the laser pulse. The rate of this (multiphoton) postionization would be strongly dependent on the intensity: for instance, under the conditions of Fig. 3 for nitrogen, it would be proportional to the fourth power of the intensity. However, the observed postionization dynamics at different distances from the beam axis suggests that the intensity dependence is substantially weaker. Therefore, in our experiments this mechanism does not work. The interaction between the generated microplasma and the probe pulse also cannot lead to an appreciable change in the electron density due to the extremely low probe radiation intensity (below 10^{10} W/cm^2).

ULTRAFAST SPECTROSCOPY OF GAS PLASMA

Along with the study of the spatiotemporal profiles of the refractive index and the electron density of the femtosecond laser microplasma, we investigated the spectral-temporal dynamics of radiation emitted by microplasma in the UV - visible spectral range. The attention was paid to the initial stage of plasma formation - from the moment of laser spark initiation (the emission of spectral continuum) to the appearance and formation of the individual spectral lines. Since the plasma emission in the form of spectral continuum sets even in the presence of the exciting laser pulse (femtosecond in our case) and the physical processes that determine the development and transformation of the continuum are characterized, generally speaking, by ultrashort (pico- and subnanosecond) times, the top priority experimental task was to develop a method for ultrafast spectral-temporal diagnostics complying with the requirements of temporal resolution and spectral responsivity. For this purpose we adopted a method for the investigation of fast processes and the recording of weak light signals which involves the use of fast streak cameras (SC). Fig. 5 shows the schematic drawing of the proposed and experimentally realized method of ultrafast spectral-temporal diagnostics of the femtosecond laser microplasma. Single pulses of Ti:Sa laser (λ=800 nm) were focused with an aspherical microlens to an intensity $I=2.5\times10^{17}$ W/cm^2 in the gases under investigation - air, nitrogen, argon, helium (at atmospheric pressure). An axially arranged concave diffraction grating formed spatially separated spectral microplasma images, which were imaged onto the SC photocathode and swept in time. The mutually perpendicular arrangement of the spectrometer dispersion plane and the SC sweep direction afforded the observation of two-dimensional spectral-temporal pictures of plasma emission.

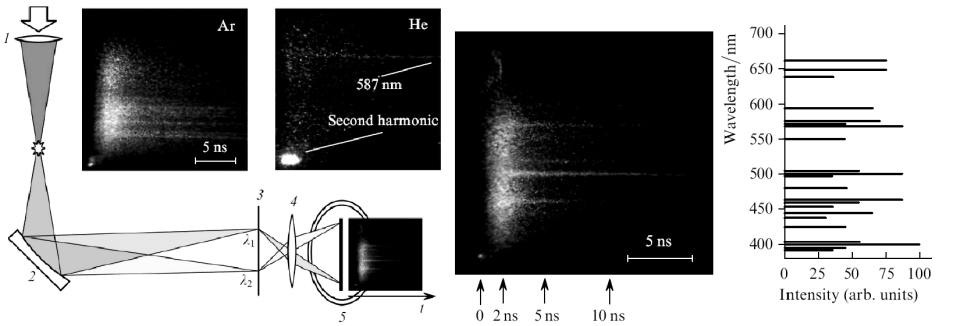

FIGURE 5. Scheme of the experiment on studying the ultrafast spectral-temporal dynamics of the femtosecond laser plasma by using a streak-camera: (1) focusing objective lens (F=8 mm, NA=0.5); (2) concave diffraction grating; (3) image plane of the diffraction grating ($\lambda_1 < \lambda_2$); (4) imaging lens; (5) streak-camera. The photos show the dynamic spectra of Ar, He and N_2 plasmas. The latter is compared with its tabulated ('statistical') line emission spectra (NIST Atomic Spectra Database, http://physics.nist.gov.PhysRefData/ASD/).

In our experiments we used a SC developed at the A.M. Prokhorov General Physics Institute, Russian Academy of Sciences [4-7]. This SC possessed a high spectral responsivity (2.1 mA/W at λ=800 nm; S1 photocathode) and a sufficiently broad

dynamic range (no less than 10), which allowed us to reliably record and study the spectral-temporal dynamics of the femtosecond plasma emission in a broad wavelength range (λ=300-1100 nm) with a temporal resolution of 2.4 ps for a sweep speed up to 5×10^9 cm/s.

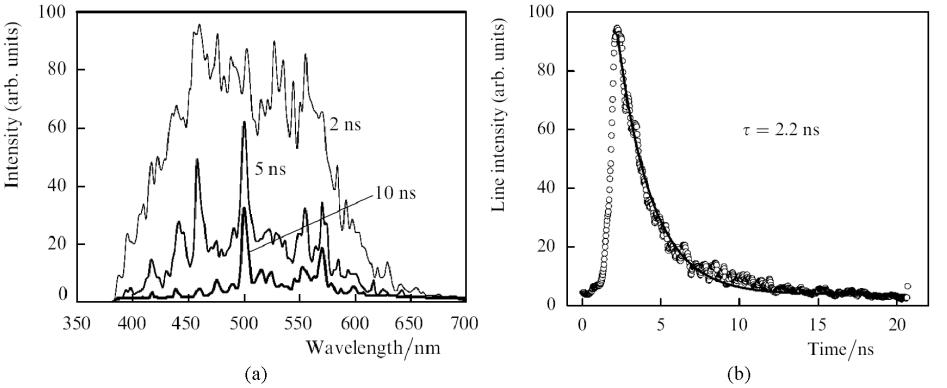

FIGURE 6. Spectral-temporal dynamics of femtosecond laser nitrogen plasma (at atmospheric pressure) in the λ=380-660 nm range. (a) - plasma emission spectra at different moment of time; (b) - time dependences of the spectral line intensity near λ=500 nm (τ is the characteristic decay time).

One can see from the data presented in Fig. 5 and Fig. 6 that the plasma emission during the initial stage of its development, which is generally rather lengthy and may last hundreds and thousands of picoseconds after the onset of plasma formation, is a spectral continuum. Individual spectral lines (at least in the visible range under investigation, λ=380-660 nm) begin to show up only several nanoseconds later, as the plasma cools down. As is emerging from the continuum, the initially broad lines narrow rapidly and change in intensity. As this takes place, some lines that are relatively intense in 'statistical' spectra are relatively weak in the dynamic plasma spectra presented. By contrast, some 'dynamically' rather bright lines hardly visible in the time-integrated spectra. This is evidently related to the existence of fast and slow radiative recombination processes in nonequilibrium plasmas. The dynamic picture of plasma spectra formation presented in Figs. 5-6 (the dynamic emission spectra of the laser-produced argon, helium and nitrogen plasmas are shown in the insets) is not only quite illustrative, but is also rather informative to serve as a substantial basis both for a qualitative and quantitative theoretical analysis of the processes occurring in the extremely nonequilibrium laser plasma. In particular, from the variation of spectral line widths one can endeavour to estimate the plasma temperature and its cooling rate, while from line intensity ratios and line decay to estimate the rates of the corresponding recombination processes. Figs. 6(b) shows the temporal intensity variation of a nitrogen spectral lines (near λ=500 nm), which decay with characteristic times τ of the order of several nanoseconds. It is evident that the absolute line intensities as well as the intensity ratios between different spectral components vary in the course of plasma development. Because a comprehensive analysis of the resultant data does not come within the province of the present paper, we only note that until the present time the pursuance of an adequate analysis of the spectra of extremely

nonequilibrium (in particular, femtosecond) laser plasmas and the ultrafast processes occurring therein has been largely limited by the lack of necessary experimental data similar to those obtained in the present work. In the preceding papers concerned with the investigation of the dynamics of the spectral composition of laser plasma emission in the visible range, the temporal resolution ranged mainly into the nano- and microseconds. This did not permit studying in detail the most interesting and least studied initial stage of plasma formation and evolution.

CONCLUSIONS

We presented the review of the recent experimental studies performed in A.M. Prokhorov General Physics Institute on fundamental mechanisms of femtosecond laser plasma dynamics. The main subject of the studies was the *micro-sized* plasma produced in gases with high intensity (up to 5×10^{17} W/cm^2), tightly focused (to a few microns in diameter) IR-UV femtosecond laser pulses. The main attention in the experiments was paid to the initial stage of microplasma formation and evolution characterized by strong laser-plasma coupling resulting in efficient ionization and heating of the medium, distortion of laser beams, and nonlinear spectral conversion of laser radiation to a continuum and laser harmonics. Using a precise pump-probe microinterferometric technique the dynamics of plasma was studied with femtosecond time-resolution in a wide density range - from a minimal detectable electron concentration (10^{19} cm^{-3}) to the almost *total* (down to nuclei) ionization of ions. The obtained time-dependences of plasma density were analyzed. It was observed, for the first time, that a characteristic time of laser plasma formation *considerably* (in times) exceeds the duration of the pump laser pulse. This *postionization* process was attributed to impact ionization of plasma by hot electrons. We compared the results of the experiments with what the theory predicted. Using an ultrafast, streak-camera-based spectroscopy technique the temporal evolution of microplasma emission and the dynamics of spectral lines formation in UV-visible range were studied with picosecond time-resolution.

REFERENCES

1. S. V. Garnov, V. I. Konov, A. A. Malyutin, O. G. Tsar'kova, I. S. Yatskovskii, F. Dausinger, *Quantum Electron.*, **33**, 758-764 (2003).
2. S. V. Garnov, V. I. Konov, A. A. Malyutin, O. G. Tsar'kova, I. S. Yatskovskii, F. Dausinger, *Laser Phys.*, **13**, 386-396 (2003).
3. V. V. Bukin, N. S. Vorob'ev, S. V. Garnov, V. I. Konov, V. I. Lozovoi, A. A. Malyutin, M. Ya. Shchelev, I. S. Yatskovskii, *Quantum Electron.*, **36**, 638-645 (2006).
4. V. V. Bukin, S. V. Garnov, A. A. Malyutin, V. V. Strelkov, *Quantum Electron.*, **37,** 961-966 (2007)
5. S. V. Garnov, V. V. Bukin, A. A. Malyutin, V. I. Konov, N. S. Vorobiev, M. Ya. Schelev, Proceedings of Int. Symp. on Topical Problems of Nonlinear Wave Physics (NWP-2005), St. Petersburg, N. Novgorod, (2005)
6. S. V. Garnov, V. I. Konov, V. I. Lozovoi, A. A. Malyutin, M. Ya. Schelev, N. S. Vorobiev, Proceedings of Int. Symp. on Modern Problems of Laser Physics (MPLP'04), Novosibirsk, (2004).
7. S. V. Garnov, V. I. Konov, V. I. Lozovoi, A. A. Malyutin, M. Ya. Schelev, N. S. Vorobiev, Proceedings SPIE Int. Soc. Opt. Eng., **5580**, 811 (2005).
8. P. Belland, C. De Michelis, M. Mattioli, *Opt. Commun.*, **3**, 7-8 (1971).

9. D. T. Attwood, L. W. Coleman, *Appl. Phys. Lett.*, **24**, 408-410 (1974).
10. H. Azechi, S. Oda, K. Tanaka, T. Norimatsu, T. Sasaki, T. Yamanaka, C. Yamanaka, *Phys. Rev. Lett.*, **39**, 1144-1147 (1977).
11. D. T. Attwood, D. W. Sweeney, J. M. Auerbach, P. H. Y. Lee, *Phys. Rev. Lett.*, **40**, 184-187 (1978).
12. D. T. Attwood, *IEEE J. Quantum Electron.*, **14**, 909-923 (1978).
13. A. Raven, O. Willi, *Phys. Rev. Lett.*, **43**, 278-282 (1979).
14. N. G. Vlasov, S. V. Korchazhkin, R. B. Matsonashvili, V. M. Petryakov, S. S. Sobolev, S. F. Chalkin, *Opt. Spektrosk.*, **59**, 934 (1985).
15. L. B. DaSilva, T. W. Barbee, R. Cauble Jr, P. Celliers, D. Ciarlo, S. Libby, R. A. London, D. Matthews, S. Mrowka, J. C. Moreno, D. Ress, J. E. Trebes, A. S. Wan, F. Weber, *Phys. Rev. Lett.*, **74**, 3991-3994 (1995).
16. Shao, Y.L., Ditmire, T., Tisch, J.W.G., Springate, E., Marangos, J.P., Hutchinson, M.H.R., "Multi-keV Electron Generation in the Interaction of Intense Laser Pulses with Xe Clusters," Phys. Rev. Lett., 77, 3343-3346 (1996).
17. G. S. Sarkisov, V. Yu. Bychenkov, V. N. Novikov, V. T. Tikhonchuk, A. Maksimchuk, S. Y. Chen, R. Wagner, G. Mourou, D. Umstadter, *Pis'ma Zh. Eksp. Teor. Fiz.*, **66**, 787 (1997).
18. T. Ditmire, E. T. Gumbrell, R. A. Smith, A. Djaoui, M. H. R. Hutchinson, *Phys. Rev. Lett.*, **80**, 720-723 (1998).
19. D. Breitling, H. Schittenhelm, P. Berger, F. Dausinger, H. Hugel, *Appl. Phys. A*, **69**, S505-S508 (1999).
20. G. S. Sarkisov, V. Yu. Bychenkov, V. N. Novikov, V. T. Tikhonchuk, A. Maksimchuk, S.-Y. Chen, R. Wagner, G. Mourou, D. Umstadter, *Phys. Rev. E*, **59**, 7042-7054 (1999).
21. M. J. Edwards, A. J. MacKinnon, J. Zweiback, K. Shigemori, D. Ryutov, A. M. Rubenchik, K. A. Keilty, E. Liang, B. A. Remington, T. Ditmire, *Phys. Rev. Lett.*, **87**, 085004 (2001).
22. A. Couairon, L. Berge, *Phys. Rev. Lett.*, **88**, 135003 (2002).
23. R. F. Smith, J. Dunn, J. Nilsen, V. N. Shlyaptsev, S. Moon, J. Filevich, J. J. Rocca, M. C. Marconi, J. R. Hunter, T. W. Barbee, *Phys. Rev. Lett.*, **89**, 065004 (2002).
24. S. V. Garnov, A. A. Malyutin, O. G. Tsarkova, V. I. Konov, F. Dausinger, Proc. SPIE Int. Soc. Opt. Eng., **4637**, 31 (2002).
25. K. Y. Kim, I. Alexeev, H. M. Milchberg, *Opt. Express*, **10**, 1563-1572 (2002).
26. H. Tang, O. Guilbaud, G. Jamelot, D. Ros, A. Klisnick, D. Joyeux, D. Phalippou, M. Kado, M. Nishikino, M. Kishimoto, K. Sukegawa, M. Ishino, K. Nagashima, H. Daido, *Appl. Phys. B*, **78**, 975-977 (2004).
27. M. Richardson, C.-S. Koay, K. Takenoshita, C. Keyser, R. Bernath, S. George, S. Teerawattansook, Proc. SPIE Int. Soc. Opt. Eng., **5580**, 434 (2005).
28. A. Giulietti, M. Galimberti, A. Gamucci, D. Giulietti, L. Gizzi, P. Koester, L. Laate, P. Tomassini, M. Vaselli, Techn. Dig. Int. Conf. on Coherent and Nonlinear Optics (ICONO/LAT'2005), St. Petersburg, (2005)
29. M. Takeda, H. Ina, S. Kobayashi, *J. Opt. Soc. Am. A*, **72**, 156-160 (1982).
30. K. Nugent, *Appl. Opt.*, **24**, 3101 (1985).
31. M. Born, E. Wolf, "Principles of Optics", Oxford, Pergamon Press, 1969; Moscow, Nauka, 1973.
32. L. D. Landau, E. M. Lifshits, "Quantum Mechanics: Non-Relativistic Theory", Oxford, Pergamon Press, 1977; Moscow, Nauka, 1989.
33. D. Bauer, P. Mulser, *Phys. Rev. A*, **59**, 569-577 (1999).
34. A. A. Balakin, G. M. Fraiman, *Zh. Eksp. Teor. Fiz.*, **93**, 695 (2001).
35. A. Brantov, W. Rozmus, R. Sydora, C. E. Capjack, V.Yu. Bychenkov, *Phys. Plasmas*, *10*, 3385 (2003).
36. G. Rascol, H. Bachau, V. T. Tikhonchuk, H.-J. Kull, T.Ristow, *Phys. Plasmas*, **13**, 103108 (2006).
37. R. A. Falk, G. Stefani, R. Camilloni, G. H. Dunn, R. A. Phaneuf, D. C. Gregory, D. H. Crandall, *Phys. Rev. A*, **28**, 91-98 (1983).
38. K. Rinn, D. C. Gregory, L. J. Wang, R. A. Phaneuf, A. Muller, *Phys. Rev. A*, **36**, 595-598 (1987).
39. R. M. Frost, P. Awakowicz, H. P. Summers, N. R. Badnell, *J. Appl. Phys.*, **84**, 2989 (1998).
40. R. U. Datla, H.-J. Kunze, *Phys. Rev. A* **37**, 4614-4619 (1998).